

Communication

Process Development of Zirconolite Ceramics for Pu Disposition: Use of a CuO Sintering Aid

Aidan A. Friskney , Ismail Aldean, Claire L. Corkhill and Lewis R. Blackburn *

Immobilisation Science Laboratory, Department of Materials Science and Engineering, University of Sheffield, Sir Robert Hadfield Building, Mappin Street, Sheffield S1 3JD, UK

* Correspondence: lewis.blackburn@sheffield.ac.uk

Abstract: Zirconolite-structured ceramics are candidate wasteform materials for the immobilisation of separated Pu. Due to the refractory properties of zirconolite and other titanates, removing residual porosity remains challenging in the final wasteform product when utilising a conventional solid state sintering route. Herein, we demonstrate that the addition of CuO as a sintering aid increases densification and promotes grain growth. Moreover, zirconolite phase formation was enhanced at lower process temperatures than typically required (≥ 1350 °C). CuO addition allowed an equivalent density to be reached using process temperatures of 250 °C lower than the undoped composition. At 150 °C lower than the undoped zirconolite, the addition of CuO resulted in a favourable microstructure and phase assemblage, as confirmed via X-ray diffraction and scanning electron microscopy. Secondary phases of CaTiO_3 and $\text{Ca}_{0.25}\text{Cu}_{0.75}\text{TiO}_3$ were observed at some processing temperatures, which may prove deleterious to wasteform performance. The use of a CuO sintering aid provides an avenue for the further development of the thermal processing of ceramic wasteform materials.

Keywords: zirconolite; ceramic; immobilisation; sintering; wasteform



Citation: Friskney, A.A.; Aldean, I.; Corkhill, C.L.; Blackburn, L.R. Process Development of Zirconolite Ceramics for Pu Disposition: Use of a CuO Sintering Aid. *Ceramics* **2023**, *6*, 678–685. <https://doi.org/10.3390/ceramics6010041>

Academic Editor: Angel L. Ortiz

Received: 11 January 2023

Revised: 14 February 2023

Accepted: 27 February 2023

Published: 8 March 2023



Copyright: © 2023 by the authors. Licensee MDPI, Basel, Switzerland. This article is an open access article distributed under the terms and conditions of the Creative Commons Attribution (CC BY) license (<https://creativecommons.org/licenses/by/4.0/>).

1. Introduction

The UK has accumulated a stockpile of separated Pu (forecast to reach 140 teHM; tonnes equivalent heavy metal) for which there is a need to develop a robust management strategy [1,2]. It is acknowledged that at least some portion of this inventory will require chemical immobilisation prior to its geological disposal; hence, there is a motive to develop, characterise and optimise the processing parameters of wasteform materials capable of immobilising Pu [3–5]. Zirconolite (ideally $\text{CaZrTi}_2\text{O}_7$) is a naturally occurring titanate mineral that has demonstrated exceptional chemical durability in both its natural analogues and synthetic derivatives and is, therefore, one of several candidate ceramic wasteform materials for separated Pu [6–13].

Conventional reactive sintering using component oxides is a common route for the fabrication of ceramic wasteform materials. Whilst the phase assemblage, density and microstructural properties of zirconolite ceramics, as a function of dopants and processing conditions, has been widely studied across a variety of discrete compositions, many samples produced by this sintering route retain moderate porosity [13–15]. Pressure-assisted sintering routes such as hot isostatic pressing (HIP) have been proposed as alternative processing routes due to an existing knowledge base from industrial practices [16–18]. A promising route to improve the densification and optimise the thermal processing cycle of wasteform materials is the use of sintering aid additives. This practice is common in relation to the fabrication of optical and electro-ceramics where porosity is deleterious to performance [19]. For example, CuO has been shown to interact with TiO_2 ceramics for dielectric applications resulting in “activated sintering”, with the CuO addition lowering the sintering temperature from 1200–1400 °C to 850–900 °C [20–22]. Given the use of TiO_2

as a precursor in the solid-state processing route of zirconolite ceramics, the CuO-TiO₂ interaction provides a possible pathway to the improved densification of these materials at a reduced sintering temperature. The aim of the present work was to investigate the effect of dilute CuO addition on the formation, microstructure and densification of the zirconolite (CaZrTi₂O₇) phase.

2. Materials and Methods

2.1. Solid State Zirconolite Fabrication

Oxide reagents CaTiO₃ (Alfa Aesar, 99.9% trace metals basis), TiO₂ -anatase (Alfa Aesar, 99.9% trace metals basis) and ZrO₂ (Alfa Aesar, 99.9% trace metals basis) were dried at 800 °C to remove adsorbed moisture and weighed in a 1:1:1 molar ratio to yield the stoichiometric zirconolite composition CaZrTi₂O₇ at a scale of 70 g. Homogenisation of the component oxides was achieved using planetary milling in a Y-ZrO₂ milling jar, with 3 mm ZrO₂ attrition media, at 400 rpm for a period of 40 min using an excess of isopropanol to act as a carrier fluid. The slurry was decanted and dried overnight at 90 °C to evaporate the excess solvent; the powder was then recovered and sieved through a 1 mm wire mesh. A selection of 2.50 g aliquots of the milled powder were then further mixed either with 2 wt. % or 5 wt. % CuO, prior to a secondary milling stage. After drying at 90 °C and powder recovery, 0.35 g of the CuO-loaded powders were uniaxially pressed into 10 mm disks before sintering in air at temperatures between 900 and 1300 °C (Δ 100 °C) for a dwell period of 20 h, with heating/cooling rates of 5 °C/min.

2.2. Materials Characterisation

Reacted samples were recovered from the furnace and ground to yield a fine powder for analysis via powder X-ray diffraction (pXRD) using a Bruker D2 Phaser. Data were collected between $5^\circ \leq 2\theta \leq 80^\circ$ using Cu K α radiation ($\lambda = 1.5406 \text{ \AA}$). Diffraction patterns were analysed using the Rietveld method to extract lattice parameters and refine quantitative phase fractions; this was achieved using the Bruker TOPAS software package [23,24]. The microstructure of polished and as-sintered surfaces was analysed using scanning electron microscopy (SEM) using either a benchtop Hitachi TM3030 operating at 15 kV with a working distance of 8 mm, fitted with a Bruker Quantax Energy Dispersive X-ray Spectrometer (EDS) for semi-quantitative compositional analysis, or an FEI Inspect f50 scanning electron microscope operating at 20 kV with a working distance of 10.6 mm. Density measurements were performed using the Archimedes method at room temperature, using ethanol as the buoyancy medium; measurements were performed five times per sample.

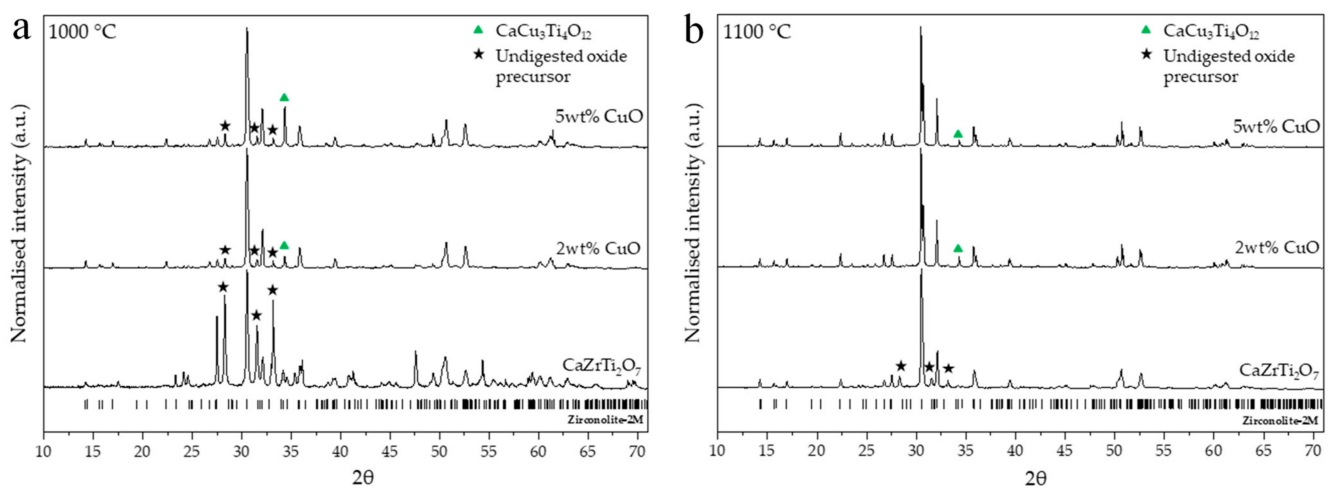
3. Results

3.1. Influence of CuO Loading on Phase Assemblage

A very low yield of the zirconolite-2M polytype was obtained when targeting a sintering temperature of 900 °C, with and without CuO loading (Table 1), with the former giving a maximum zirconolite yield of 30.5(5) wt.% with 2 wt.% CuO loading. When synthesised at 1000 °C, the addition of CuO caused a significant increase in the proportion of the zirconolite phase formed, as summarised in Figure 1a; however, characteristic reflections for the constituent CaTiO₃, ZrO₂ and TiO₂ phases remained detectable at all CuO loadings, demonstrating that the reaction to form zirconolite remained incomplete at this temperature. Rietveld analysis of the powder XRD data indicated that zirconolite-2M comprised only 35.2(4) wt.% of the overall phase assemblage with no CuO additive at 1000 °C, whereas a yield of 86.5(2) wt.% was obtained with the addition of 2 wt.% CuO.

Table 1. Zirconolite phase fraction as a function of sintering temperature determined from Rietveld analysis of p-XRD data.

Nominal Composition	Sintering Temperature (°C)	Phase Fraction (wt.%)				
		Zirconolite 2M	CaTiO ₃	CaCu ₃ Ti ₄ O ₁₂	ZrO ₂	TiO ₂
CaZrTi ₂ O ₇	900	25.6 (30)	29.5 (12)	-	28.2 (11)	16.8 (21)
+2 wt.% CuO	900	30.5 (5)	25.1 (3)	3.5 (2)	26.7 (3)	14.3 (2)
+5 wt.% CuO	900	27.8 (6)	23.7 (3)	9.9 (2)	27.1 (3)	11.5 (2)
CaZrTi ₂ O ₇	1000	35.2 (4)	25.4 (3)	-	25.5 (2)	13.9 (2)
+2 wt.% CuO	1000	86.5 (2)	4.5 (2)	3.0 (1)	6.0 (1)	-
+5 wt.% CuO	1000	80.4 (2)	4.4 (1)	9.5 (1)	5.8 (1)	-
CaZrTi ₂ O ₇	1100	81.6 (5)	5.6 (2)	-	8.4 (2)	4.4 (4)
+2 wt.% CuO	1100	95.8 (3)	2.4 (3)	1.8 (1)	-	-
+5 wt. % CuO	1100	93.3 (3)	2.6 (3)	4.2 (2)	-	-
CaZrTi ₂ O ₇	1200	93.2 (16)	-	-	6.8 (5)	-
+2 wt.% CuO	1200	99.1 (1)	-	0.8 (1)	-	-
+5 wt.% CuO	1200	96.6 (1)	-	3.3 (1)	-	-
CaZrTi ₂ O ₇	1300	100 (0)	-	-	-	-
+2 wt.% CuO	1300	97.0 (2)	2.0 (2)	1.0 (1)	-	-
+5 wt.% CuO	1300	93.6 (2)	2.3 (1)	4.1 (1)	-	-

**Figure 1.** Powder X-ray diffraction data obtained for compositions synthesised at (a) 1000 °C and (b) 1100 °C. CaCu₃Ti₄O₁₂ characteristic reflections are highlighted with green triangles and precursor phase reflections are highlighted with black stars.

A secondary CaCu₃Ti₄O₁₂ phase was also stabilised at low concentrations in the zirconolites loaded with CuO, characterised by the reflection at $2\theta = 32.05^\circ$ in Figure 1b; however, in both the 2 and 5 wt.% CuO samples, the accompanying fraction of this phase appeared to decrease with an elevated sintering temperature of 1100 °C. Rietveld analysis (summarised in Table 1) demonstrated that some secondary CaCu₃Ti₄O₁₂, as well as CaTiO₃, were retained in the CuO-doped materials processed at 1300 °C, preventing these compositions from forming a single-phase product. Across the entire temperature range, the 5 wt.% CuO compositions consistently demonstrated a lower zirconolite-2M phase fraction relative to 2 wt.% CuO (Figure 2) This was considered to be the result of the higher CuO content stabilising a greater proportion of the CaCu₃Ti₄O₁₂ phase, indicating that 2 wt.% CuO was sufficient to achieve advantageous processing effects while suppressing the formation of Cu-bearing secondary phases.

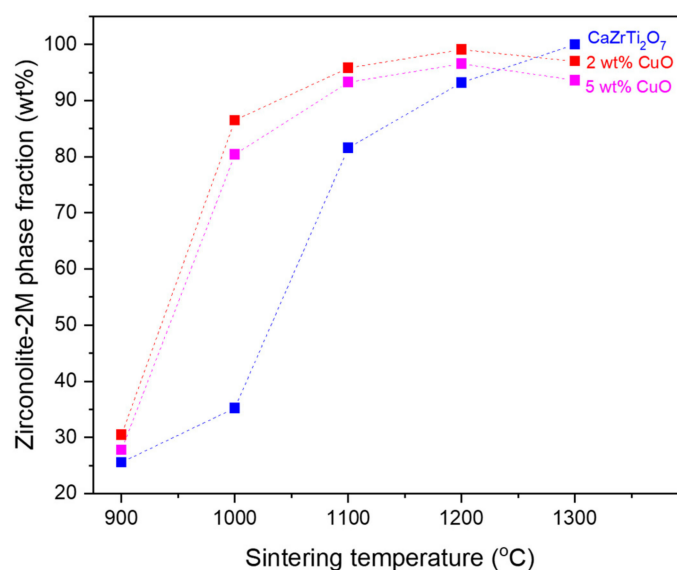


Figure 2. Zirconolite-2M phase fractions obtained from Rietveld analysis of powder XRD data.

3.2. Microstructure and Density

Alongside the successful formation of the target zirconolite phase, a primary motive for deploying the CuO sintering aid was to assist densification at reduced temperatures and reduce the retained porosity in the final product, as this will impact the specific surface area available for leaching in the disposal environment [25]. The microstructure of the CuO-loaded zirconolite was analysed using SEM using polished specimens, as shown in Figure 3. When compared to a sample of CaZrTi₂O₇ processed at 1350 °C with no CuO, a marked reduction in porosity was observed in the compositions loaded with 2 wt.% CuO when processed at 1200 and 1300 °C. When targeting 5 wt.% CuO at 1200 °C, a Cu-rich grain boundary phase was also observed with a slightly brighter contrast than the bulk zirconolite phase, consistent with the CaCu₃Ti₄O₁₂ phase identified using XRD analysis. A decrease in retained porosity was consistent with an increased product density; for example, the baseline CaZrTi₂O₇ product synthesised at 1200 °C had a density of 4.18(6) g/cm³ (Table 2). This was observed to increase to 4.31(3) g/cm³ with 5 wt. % CuO loading. The surfaces of the as-sintered specimens were also analysed using SEM to determine the influence of CuO loading on the obtained phase assemblage and microstructure (Figure 4). When sintering CaZrTi₂O₇ at 1000 °C, the microstructure was poorly sintered. Strong variations in backscattered electron contrast and obvious changes in morphology were indicative of an incomplete reaction, consistent with the XRD analysis. The effect of 2 wt.% CuO addition at 1000 °C was significant, with a significant reduction in the observable porosity (Figure 4b), in addition to a marked decrease in the quantity of component oxides and an increase in density from 3.81(55) to 4.18(6) g/cm³ (although the large uncertainty associated with the un-doped density should be noted). An increase in both grain size and density was observed with 2 wt.% CuO at both 1100 and 1200 °C (Figure 4c–f); although, the presence of the secondary CaTiO₃ and CaCu₃Ti₄O₁₂ phases was clearly resolved. The stabilisation of secondary perovskite phases is considered undesirable on the basis of reduced chemical durability relative to the target zirconolite phase [26]. EDS analysis of the individual phases present in the specimen of CaZrTi₂O₇ with 5 wt.% CuO sintered at 1300 °C is presented in Figure 5. Three distinct phases were resolved, consistent with powder XRD analysis and complementary Rietveld analysis, corresponding to approximately 2.33 and 4.05 wt.% CaTiO₃ and CaCu₃Ti₄O₁₂, respectively. The EDS spectra were used to reliably identify each phase, demonstrating that the Cu-rich CaCu₃Ti₄O₁₂ was preferentially distributed at the boundaries between CaZrTi₂O₇ grains.

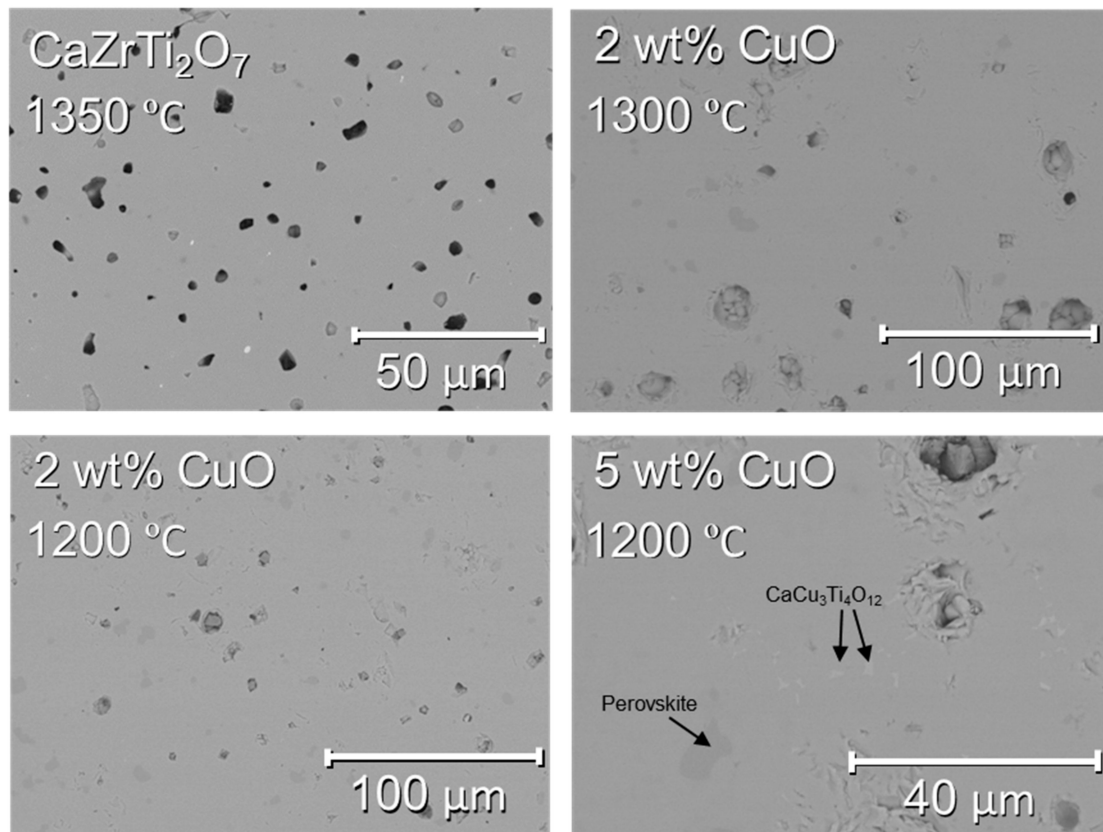


Figure 3. BSE-SEM micrographs demonstrating the effect of CuO addition on the density and phase assemblage of CuO-loaded zirconolite materials.

Table 2. Archimedes density data obtained for $\text{CaZrTi}_2\text{O}_7$ samples. Errors quoted are the standard deviation of five separate measurements performed for each sample. Relative density is based on the calculated density of $\text{CaZrTi}_2\text{O}_7$ (4.44 g/cm^3).

Nominal Composition	Sintering Temperature (°C)	Archimedes Density (g/cm^3)	Relative Density
$\text{CaZrTi}_2\text{O}_7$	1100	3.81(55)	85.8(124)
$\text{CaZrTi}_2\text{O}_7 + 2 \text{ wt.}\% \text{ CuO}$	1100	4.18(6)	94.1(14)
$\text{CaZrTi}_2\text{O}_7 + 5 \text{ wt.}\% \text{ CuO}$	1100	4.18(2)	94.1(4)
$\text{CaZrTi}_2\text{O}_7$	1200	4.18(6)	94.1(14)
$\text{CaZrTi}_2\text{O}_7 + 2 \text{ wt.}\% \text{ CuO}$	1200	4.24(4)	95.5(9)
$\text{CaZrTi}_2\text{O}_7 + 5 \text{ wt.}\% \text{ CuO}$	1200	4.31(3)	97.1(7)
$\text{CaZrTi}_2\text{O}_7$	1300	4.21(12)	94.8(27)
$\text{CaZrTi}_2\text{O}_7 + 2 \text{ wt.}\% \text{ CuO}$	1300	4.27(3)	96.2(7)
$\text{CaZrTi}_2\text{O}_7 + 5 \text{ wt.}\% \text{ CuO}$	1300	4.25(3)	95.7(7)

The mechanism by which the CuO additive improved the densification of zirconolite, at reduced sintering temperatures, was considered to be the result of a CuO-TiO₂ eutectic that has been previously characterised to promote liquid phase formation in ceramic samples above 1000 °C [22]. The composition of this eutectic is approximately 83CuO:17TiO₂, meaning that any eutectic liquid formed will be very rich in CuO. EDS analysis (Figure 5) of the $\text{CaZrTi}_2\text{O}_7 + 5 \text{ wt.}\% \text{ CuO}$ material sintered at 1300 °C clearly identified a Cu-rich grain boundary phase consistent with a Cu-rich melt in CuO additive samples. This interaction appeared to begin at 1000 °C, as evidenced by a marked increase in the yield of the zirconolite-2M phase, and was not observed in the materials processed at 900 °C, corresponding to the temperature at which the CuO-TiO₂ eutectic interaction has been reported to occur in the literature [22].

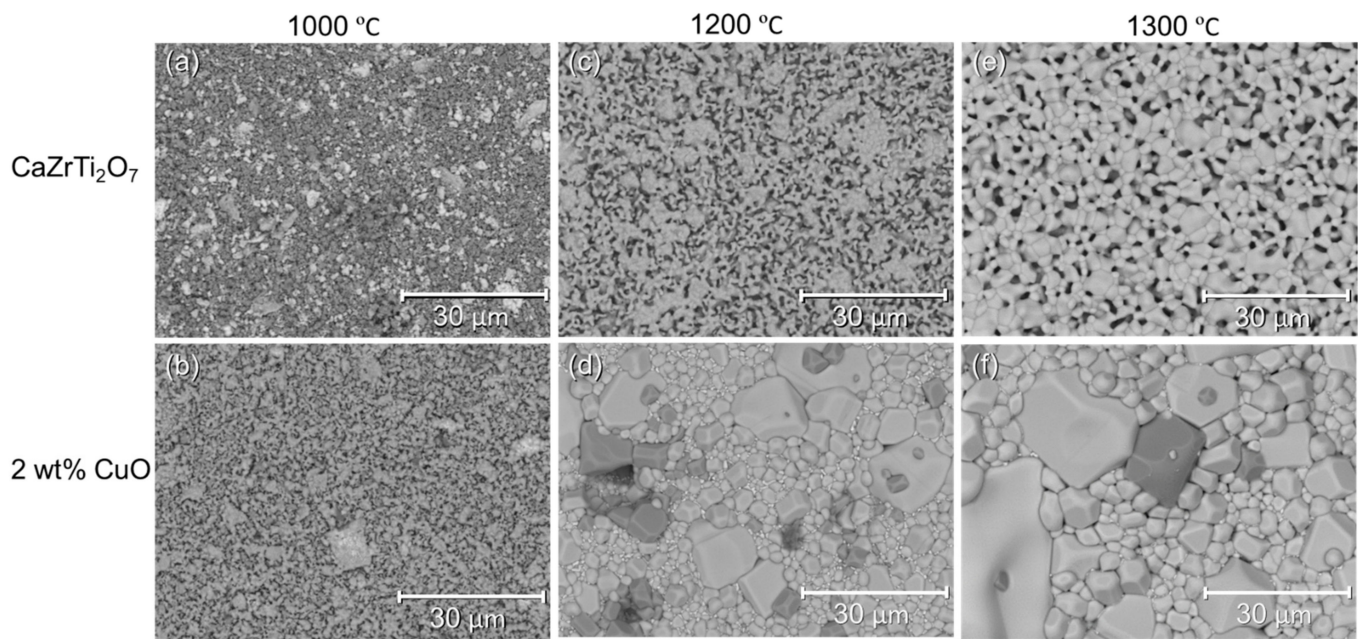


Figure 4. Scanning electron micrographs of (a) undoped CaZrTi₂O₇ sintered at 1000 °C; (b) 2 wt.% CuO sintered at 1000 °C; (c) undoped CaZrTi₂O₇ sintered at 1200 °C; (d) 2 wt.% CuO sintered at 1200 °C; (e) undoped CaZrTi₂O₇ sintered at 1300 °C; (f) 2 wt.% CuO sintered at 1300 °C.

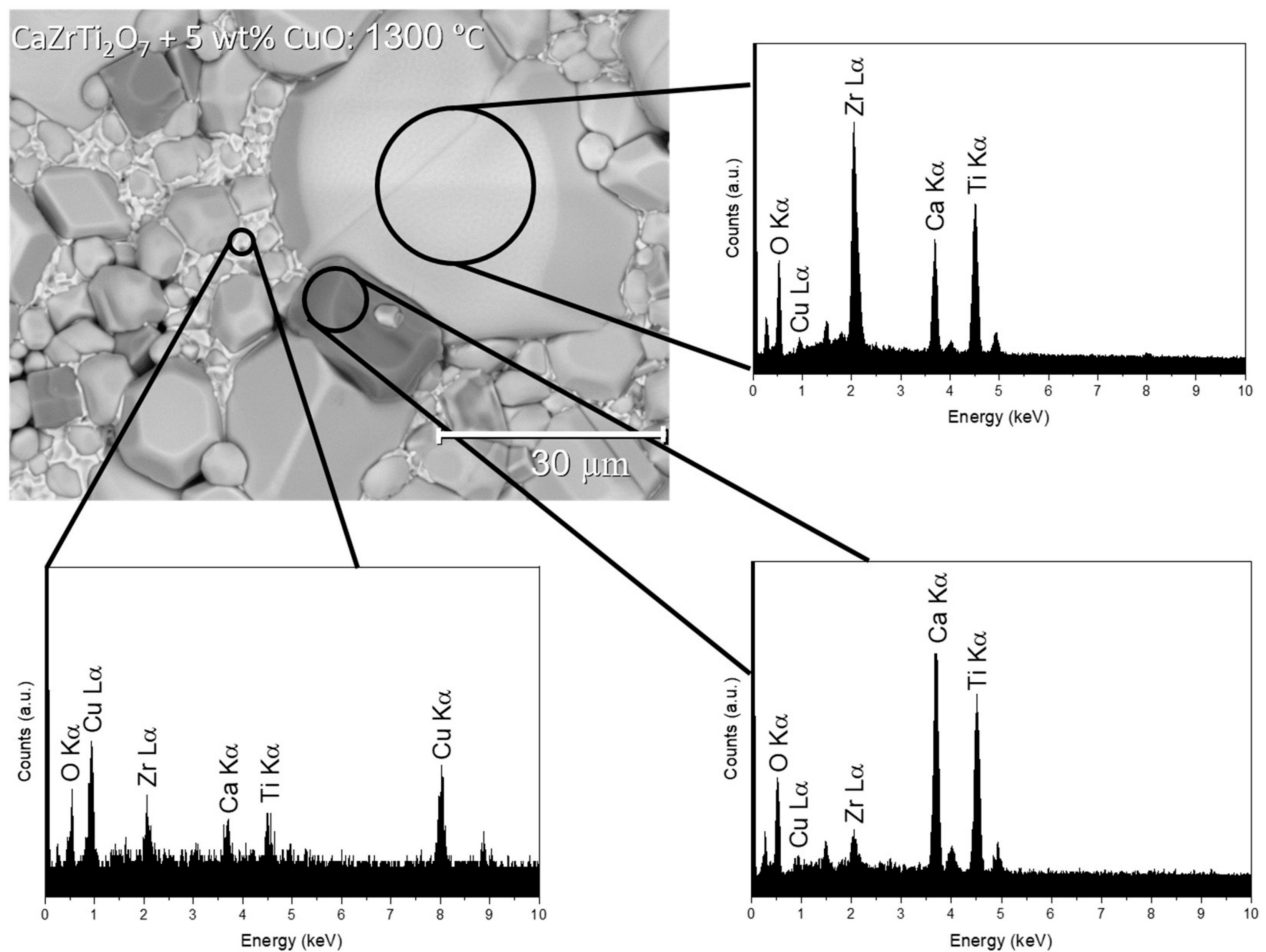


Figure 5. SEM/EDS analysis of CaZrTi₂O₇ + 5 wt.% CuO sintered at 1300 °C.

4. Conclusions

The use of CuO as a sintering aid was investigated for improving the densification of CaZrTi₂O₇ zirconolite and lowering processing temperatures. The addition of CuO generally improved the formation yield of the zirconolite phase as well as improving densification. The improvement to phase assemblage began at 1000 °C and this was attributed to the formation of a CuO/TiO₂ eutectic liquid that assists the diffusion of species required to form the zirconolite phase. Grain growth was then assisted at 1100 and 1200 °C, resulting in improvements to microstructure properties and densification. A secondary CaCu₃Ti₄O₁₂ phase was obtained to a lesser extent in the 2 wt.% CuO-loaded material relative to the 5 wt.% formulations and, therefore, 2 wt.% CuO appeared to be a more favourable upper limit of the additive concentration. The most favourable compromise between phase assemblage, reduced processing temperature and improved densification was considered to be achieved at 1200 °C with 2 wt.% CuO. Further development of atmospheric processing conditions is required to achieve phase pure zirconolite in the simulat wasteform. These data form a promising basis from which the application of the CuO additive, and other commercially available sintering aids, could be applied to more representative wasteform compositions containing a Pu surrogate fraction.

Author Contributions: A.A.F.: Investigation, formal analysis, visualisation, writing—original draft. I.A.: Investigation, formal analysis. C.L.C.: Conceptualisation, project administration, funding acquisition, methodology, supervision, writing—review and editing. L.R.B.: Conceptualisation, validation, visualization, methodology, supervision, writing—review and editing. All authors have read and agreed to the published version of the manuscript.

Funding: This research was part-funded by the Nuclear Decommissioning Authority and EPSRC under grant codes EP/S022295/1, EP/T517835/1, EP/N017374/1, EP/T011424/1.

Data Availability Statement: The data that support these findings cannot be shared at the present time as they form part of an ongoing study.

Acknowledgments: The authors are grateful to the Nuclear Decommissioning Authority for part-funding this work through the award of a PhD bursary, as part of the EPSRC GREEN Centre for Doctoral Training (EP/S022295/1). L. R. Blackburn and C. L. Corkhill wish to acknowledge EPSRC for fellowship funding, under grant awards EP/T517835/1 and EP/N017374/1. This research utilized the HADES/MIDAS facility at the University of Sheffield established with financial support from EPSRC and BEIS, under grant EP/T011424/1 [27].

Conflicts of Interest: The authors declare no conflict of interest. The funders had no role in the design of the study; in the collection, analyses, or interpretation of data; in the writing of the manuscript; or in the decision to publish the results.

References

1. Hyatt, N.C. Plutonium management policy in the United Kingdom: The need for a dual track strategy. *Energy Policy* **2017**, *101*, 303–309. [CrossRef]
2. Hyatt, N.C. Safe management of the UK separated plutonium inventory: A challenge of materials degradation. *NPJ Mater. Degrad.* **2020**, *4*, 28. [CrossRef]
3. *NDA Report—SMS/TS/B1-PLUT/002/A, Plutonium Credible Options Analysis (Gate A)*; Nuclear Decommissioning Authority: Risley, UK, 2010.
4. Hobbs, J.W.; Scales, C.; Maddrell, E.R.; Stewart, M.W.A.; Moricca, S.A. A programme to immobilise plutonium residues at Sellafield. In Proceedings of the 53rd Annual Institute of Nuclear Materials Management (INMM), Orlando, FL, USA, 15–19 July 2012.
5. Thornber, S.M.; Jovanovic, M.; Davis, J.; Vance, E.R.; Gregg, D.; Chavara, D.T.; Watson, I.; Stennett, M.C.; Hyatt, N.C. A preliminary validation study of PuO₂ incorporation into zirconolite glass-ceramics. *MRS Adv.* **2018**, *3*, 1065–1071. [CrossRef]
6. Lumpkin, G.R.; Whittle, K.R.; Howard, C.; Zhang, Z.; Berry, F.J.; Oates, G.; Williams, C.T.; Zaitsev, A.N. Crystal Chemistry and Cation Ordering in Zirconolite 2M. In *MRS Online Proceedings Library (OPL)*; Cambridge University Press: Cambridge, UK, 2006; Volume 932.
7. Ringwood, A.E.; Kesson, S.E.; Ware, N.G.; Hibberson, W.; Major, A. Immobilisation of high level nuclear reactor wastes in SYNROC. *Nature* **1979**, *278*, 219–223. [CrossRef]

8. Blackburn, L.R.; Sun, S.; Gardner, L.J.; Maddrell, E.R.; Stennett, M.C.; Hyatt, N.C. A systematic investigation of the phase assemblage and microstructure of the zirconolite $\text{CaZr}_{1-x}\text{Ce}_x\text{Ti}_2\text{O}_7$ system. *J. Nucl. Mater.* **2020**, *535*, 152137. [[CrossRef](#)]
9. Vance, E.R.; Lumpkin, G.R.; Carter, M.L.; Cassidy, D.J.; Ball, C.J.; Day, R.A.; Begg, B.D. Incorporation of Uranium in Zirconolite ($\text{CaZrTi}_2\text{O}_7$). *J. Am. Ceram. Soc.* **2002**, *85*, 1853–1859. [[CrossRef](#)]
10. Vance, E.R.; Ball, C.J.; Day, R.A.; Smith, K.L.; Blackford, M.G.; Begg, B.D.; Angel, P.J. Actinide and rare earth incorporation into zirconolite. *J. Alloys Compd.* **1994**, *213/214*, 406–409. [[CrossRef](#)]
11. Begg, B.D.; Day, R.A.; Brownscombe, A. Structural Effect of Pu substitutions on the Zr site in Zirconolite. *Mater. Res. Soc. Symp. Proc.* **2001**, *663*, 259. [[CrossRef](#)]
12. Begg, B.D.; Vance, E.R.; Conradson, S.D. The Incorporation of Plutonium and Neptunium in Zirconolite and Perovskite. *J. Alloys Compd.* **1998**, *271–273*, 221–226. [[CrossRef](#)]
13. Blackburn, L.R.; Sun, S.; Lawson, S.M.; Gardner, L.J.; Ding, H.; Corkhill, C.L.; Maddrell, E.R.; Stennett, M.C.; Hyatt, N.C. Synthesis and Characterisation of $\text{Ca}_{1-x}\text{Ce}_x\text{ZrTi}_{2-2x}\text{Cr}_2\text{O}_7$: Analogue Zirconolite Wasteform for the Immobilisation of Stockpiled UK Plutonium. *J. Eur. Ceram. Soc.* **2020**, *40*, 5909–5919. [[CrossRef](#)]
14. Blackburn, L.R.; Sun, S.K.; Gardner, L.J.; Maddrell, E.R.; Stennett, M.C.; Corkhill, C.L.; Hyatt, N.C. Synthesis, structure, and characterization of the thorium zirconolite $\text{CaZr}_{1-x}\text{Th}_x\text{Ti}_2\text{O}_7$ system. *J. Am. Ceram. Soc.* **2021**, *104*, 2937–2951. [[CrossRef](#)]
15. Zhong, M.-X.; Walkley, B.; Bailey, D.J.; Blackburn, L.R.; Ding, H.; Wang, S.-Q.; Bao, W.-C.; Gardner, L.J.; Sun, S.-K.; Stennett, M.C.; et al. Synthesis of $\text{Ca}_{1-x}\text{Ce}_x\text{ZrTi}_{2-2x}\text{Al}_{2x}\text{O}_7$ zirconolite ceramics for plutonium disposition. *J. Nucl. Mater.* **2021**, *556*, 153198. [[CrossRef](#)]
16. Blackburn, L.R.; Gardner, L.J.; Sun, S.K.; Maddrell, E.R.; Stennett, M.C.; Corkhill, C.L.; Hyatt, N.C. Hot Isostatically Pressed Zirconolite Wasteforms for Actinide Immobilisation. In Proceedings of the IOP Conference Series: Materials Science and Engineering, Manchester, UK, 10–13 September 2020; Volume 818.
17. Blackburn, L.R.; Cole, M.R.; Gardner, L.J.; Bailey, D.J.; Kuman, M.; Mason, A.R.; Sun, S.K.; Maddrell, E.R.; Stennett, M.C.; Corkhill, C.L.; et al. Synthesis and characterisation of HIP $\text{Ca}_{0.80}\text{Ce}_{0.20}\text{ZrTi}_{1.60}\text{Cr}_{0.40}\text{O}_7$ zirconolite and observations of the ceramic–canister interface. *MRS Adv.* **2021**, *6*, 112–116. [[CrossRef](#)]
18. Zhang, Y.; Stewart, M.W.A.; Li, H.; Carter, M.L.; Vance, E.R.; Moricca, S. Zirconolite-rich titanate ceramics for immobilisation of actinides—Waste form/HIP can interactions and chemical durability. *J. Nucl. Mater.* **2009**, *395*, 69–74. [[CrossRef](#)]
19. Hostaša, J.; Picelli, F.; Hřibalová, S.; Nečina, V. Sintering aids, their role and behaviour in the production of transparent ceramics. *Open Ceram.* **2021**, *7*, 100137. [[CrossRef](#)]
20. Meng, F. Influence of sintering temperature on semi-conductivity and nonlinear electrical properties of TiO_2 -based varistor ceramics. *Mater. Sci. Eng. B* **2005**, *117*, 77–80. [[CrossRef](#)]
21. Chang, J.-C.; Chen, Y.-F.; Jean, J.-H. Low-fire processing and dielectric properties of TiO_2 with MnO_x -CuO. *Jpn. J. Appl. Phys.* **2004**, *43*, 4267. [[CrossRef](#)]
22. Nie, J.; Chan, J.M.; Qin, M.; Zhou, N.; Luo, J. Liquid-like grain boundary complexation and sub-eutectic activated sintering in CuO-doped TiO_2 . *Acta Mater.* **2017**, *130*, 329–338. [[CrossRef](#)]
23. Coelho, A.A. Whole-profile structure solution from powder diffraction data using simulated annealing. *J. Appl. Crystallogr.* **2000**, *33*, 899–908. [[CrossRef](#)]
24. Coelho, A.A. A charge-flipping algorithm incorporating the tangent formula for solving difficult structures. *Acta Crystallogr. Sect. A Found. Crystallogr.* **2007**, *63*, 400–406. [[CrossRef](#)]
25. Blackburn, L.R.; Bailey, D.J.; Sun, S.; Gardner, L.J.; Martin, M.C.; Corkhill, C.L.; Hyatt, N.C. Review of zirconolite crystal chemistry and aqueous durability. *Adv. Appl. Ceram.* **2021**, *120*, 69–83. [[CrossRef](#)]
26. Blackburn, L.R.; Crawford, R.; Walling, S.A.; Gardner, L.J.; Cole, M.R.; Sun, S.; Gausse, C.; Mason, A.R.; Stennett, M.C.; Maddrell, E.R.; et al. Influence of accessory phases and surrogate type on accelerated leaching of zirconolite wasteforms. *NPJ Mater. Degrad.* **2021**, *4*, 28. [[CrossRef](#)]
27. Hyatt, N.C.; Corkhill, C.L.; Stennett, M.C.; Hand, R.J.; Gardner, L.J.; Thorpe, C.L. The HADES Facility for High Activity Decommissioning Engineering & Science: Part of the UK National Nuclear User Facility. In Proceedings of the IOP Conference Series: Materials Science and Engineering, 2020; Volume 818, pp. 1–8.

Disclaimer/Publisher’s Note: The statements, opinions and data contained in all publications are solely those of the individual author(s) and contributor(s) and not of MDPI and/or the editor(s). MDPI and/or the editor(s) disclaim responsibility for any injury to people or property resulting from any ideas, methods, instructions or products referred to in the content.